Eur. Phys. J. B **32**, 157–161 (2003)
DOI: 10.1140/epjb/e2003-00084-8

THE EUROPEAN PHYSICAL JOURNAL B

Er^{3+}–Li^{+} ion exchange in lithium niobate crystals: an EXAFS study

S. Padovani[1], F. D'Acapito[2], C. Sada[1,a], E. Cattaruzza[3], F. Gonella[3], N. Argiolas[1], M. Bazzan[1], C. Maurizio[1], and P. Mazzoldi[1]

[1] INFM and Dipartimento di Fisica, Università di Padova, Via Marzolo 8, 35131 Padova, Italy
[2] INFM and ESRF-GILDA CRG, BP 220, 38043 Grenoble, France
[3] INFM and Dipartimento di Chimica Fisica, Università di Venezia, Dorsoduro 2137 30123 Venezia, Italy

Received 21 November 2002
Published online 1st April 2003 –

Abstract. Lithium niobate crystals doped with erbium by the ion exchange process were studied by means of extended X-ray absorption fine structure spectroscopy and secondary ion mass spectrometry. The study of the local atomic order allowed the determination of the erbium environment in the crystal matrix and the investigation on the role of preparation conditions.

PACS. 82.39.Wj Ion exchange, dialysis, osmosis, electro-osmosis, membrane processes – 77.84.Dy Niobates, titanates, tantalates, PZT ceramics, etc. – 61.10.Ht X-ray absorption spectroscopy: EXAFS, NEXAFS, XANES, etc.

1 Introduction

The exploding demand for Internet access, telecommunications and broadband service has led to a push for a greater lightwave transmission capacity forbidden to electrical technology. As a consequence, an increasing impulse toward the development of new materials for generation, guiding, switching and amplification of light compatible with the planar geometry is constantly given. In particular, the optical communication technology has been largely interested in materials able to host rare earths and, especially, erbium due to its well-known key role in the optical signal amplification for the 1.55 μm telecommunications wavelength. In this scenario, the combination of excellent electro-optical, acousto-optical and nonlinear optical properties makes lithium niobate ($LiNbO_3$) an attractive host material for application in integrated optoelectronics technology. As a matter of fact, the promising results reported in literature [1–6] so far opened the way to new challenges, namely the employment of new low-cost and high-reliable techniques for local doping of $LiNbO_3$ crystals which maintain full compatibility with the planar geometry. Among them, ion exchange is a promising candidate since few years ago the feasibility of erbium local doping of lithium niobate by ion exchange technique was demonstrated [6,7]. The systematic analysis on the role of the preparation conditions was later reported [8,9] and evidenced that location of erbium ions in the lattice is critical for optimising the optical response of the doped $LiNbO_3$. As a matter of fact, the gain response of an active element is strongly influenced by the crystalline field generated by the surrounding environment at the dopant site. Consequently, the presence of different locations in the matrix corresponds to a broadening in the spectral response and to a possible modification in the lifetimes. Since the knowledge of the lattice position of the impurities is mandatory for understanding the microscopic processes induced by the dopant incorporation [10] and to optimise the process, we decided to exploit the extended X-ray absorption fine structure spectroscopy (EXAFS) to study the erbium local environment.

In this work, the EXAFS study is performed by collecting the signal in both the x-ray fluorescence yield (XFY) and total electron yield (TEY) modes [11] at Er L_{III}-edge for a set of selected samples. In the former case the EXAFS sampling depth covers the full exchanged region while in the second case, only the outmost layer (about two hundreds nm thick) can be investigated. The study of the erbium local environment has been combined to the compositional analysis in order to connect the diffusion and exchange behavior with the location detected by EXAFS. Moreover, the comparison of these results with the erbium in- depth profiles allows the relation of both the local environment and the site occupied by erbium atoms embedded in the matrix with the various preparation conditions.

2 Experimental procedures

The ion exchange process was obtained by immersing the lithium niobate crystals (both X- and Z-cut) in a molten

[a] e-mail: sada@padova.infm.it

Table 1. Ion exchange parameters.

Sample	Cut	heating rate	exchange temperature	exchange time	$Er_2(SO_4)_3$ wt%
S56Z	Z	100 °C/h	600 °C	40 h	0.18%
S50Z	Z		645 °C	15 h	0.18%
S58Z	Z		645 °C	40 h	0.18%
H2X	X	300 °C/h	560 °C	24 h	4.7%
H4X	X		600 °C	7 h	0.1%
H4Z	Z		600 °C	7 h	0.1%

eutectic solution of Li_2SO_4, Na_2SO_4 and K_2SO_4, in the proportion of 70.7, 9.9 and 19.4 wt.%, respectively, with the addition of a small amount of $Er_2(SO_4)_3$, ranging from 0.005 to 5 wt.%. The amount of lithium ions in the bath composition limited the loss of this ion species from the lithium niobate crystal [6]. Table 1 summarizes the details of the preparation conditions employed in this investigation, *i.e.* the processing time and temperature, the erbium sulphate content added to the starting bath, and the heating rate used to melt it.

EXAFS measurements were performed at the European Synchrotron Radiation Facility (ESRF) on the Italian beamline GILDA, with a bending magnet device source. The sagittally focusing monochromator, used in the so-called dynamical focusing mode [12], was equipped with two Si (311) crystals. The flux on the sample was of the order of 1×10^{10} photons s^{-1} on a 2 mm spot size. EXAFS spectra were collected at Er L_{III}-edge, cooling the samples at liquid nitrogen temperature; due to low Er concentration in the samples, the X-ray absorption spectra were collected in fluorescence mode (XFY), by a high-purity 7-element Ge detector. In this configuration the EXAFS spectra take contribution from the whole Er-doped region. The X-ray absorption coefficient was also measured for some samples in total electron yield mode (TEY) with a channeltron detector, in order to probe the shallower part of the doped zone. Er L_{III}-edge X-ray absorption spectrum of Er_2O_3 crystalline powder was measured at liquid nitrogen temperature in transmission mode as a reference sample. Data processing was carried out by Fourier filtering and multi-parameter fit in the R-space of the first coordination shell. Theoretical scattering amplitude and phase for the Er-O coordination were generated by FEFF8 code [13] using the structure of crystalline Er_2O_3. The multi-electron amplitude reduction factor S_0^2 in standard EXAFS formula was fixed to the value obtained from the Er_2O_3 EXAFS spectrum ($S_0^2 = 1.0 \pm 0.1$).

Compositional analysis was performed by means of secondary ion mass spectrometry (SIMS) using an IMS-4f CAMECA spectrometer equipped with a normal incidence electron gun used to compensate the surface charge build-up while profiling insulating samples such as $LiNbO_3$ crystals. Compositional profiles were obtained using 14.5 keV Cs^+ bombardment and negative secondary ion detection (primary beam intensity: 50 nA; rastered area: 125×125 μm^2). The erosion speed was evaluated by measuring the depth of the crater at the end of each analysis by a step profilometer (Tencor Alpha).

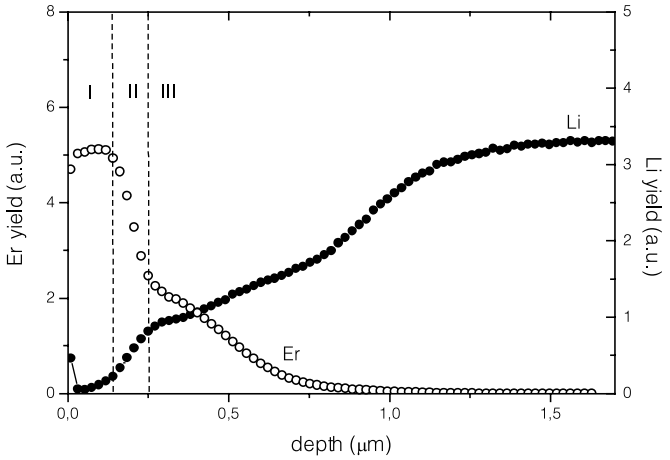

Fig. 1. Erbium and lithium SIMS profiles (H2X sample). Ion exchange parameters: $T = 560$ °C, $t = 24$ h, $Er_2(SO_4)_3 = 4.7$ wt.%, 300 °C/h heating ramp.

3 Results and discussion

In the following we report the results of both SIMS and EXAFS analyses.

3.1 SIMS analysis

The compositional analysis performed by SIMS technique confirmed that, independently of the process parameters, the doping process can be explained in terms of erbium-lithium exchange mechanism. Nb does not take part to the process: the lithium depletion, in fact, corresponds exactly to Er in-diffusion, as clearly shown in Figures 1 and 2 where erbium and lithium profiles are reported for a fast (300 °C/h) and slow (100 °C/h) heating rates, respectively. The heating rate used to melt the starting bath demonstrated to be the most critical parameter since it strongly affects both the optical quality of the crystals [9] and the dynamics of erbium incorporation in the substrate. As a matter of fact, the samples obtained with a fast heating rate exhibits surface opacity which, on the contrary, can be prevented lowering the heating rate down to 100 °C/h independently of the other process parameters. The main experimental findings are:

- when a fast heating rate is used, Er incorporation is the results of two different dynamics processes: the first mainly interests the surface (of the order of 0.1–0.2 μm thick) and creates a sort of Er reservoir. The second is more easily explained by a in-diffusion process of the dopant ions provided by the surface nearby layer. These two distinct regions are separated by a transition layer in which the concentration gradient of both erbium and lithium atoms is very high (see Fig. 1) [7,8].
- When a slow heating rate (100 °C/h) is used, the distinct regions previously mentioned are not observed (see Fig. 2). The erbium in-depth profile is closer to that expected in the case of a diffusive regime.

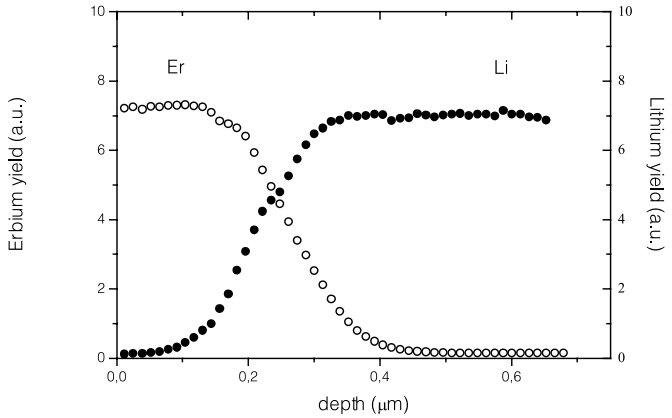

Fig. 2. Erbium and lithium SIMS profiles (S56Z sample). Ion exchange parameters: $T = 600$ °C, $t = 40$ h, $Er_2(SO_4)_3 = 0.18$ wt.%, 100 °C/h heating ramp.

– The other process parameters, *i.e.* erbium sulphate percentages in the starting bath, processing time and temperature, mainly influence the total erbium concentration and the final exchanged layer thickness [14].
– The exchange process is anisotropic, the erbium is deeply incorporated in the X-cut crystals with respect the Z-cut one.

3.2 EXAFS analysis

The EXAFS study was performed to clarify whether the different process dynamics of erbium incorporation is accompanied by a variation on the local environment of erbium ions in the matrix when different heating rates are employed.

3.2.1 X-ray fluorescence yield detection mode

In Figure 3 the EXAFS spectra of the ion-exchanged samples, collected in fluorescence mode, are reported together with the Er_2O_3 standard one, all taken at the Er L_{III}-edge. The Figure 4 shows the corresponding k^3-weighted Fourier transform moduli in the 2–9 $Å^{-1}$ k-range. Independently of the preparation conditions, the experimental data exhibit both a peak located at about 2 Å, corresponding to coordination with oxygen atoms, and a lower signal around 3–4.5 Å. The fitting results for the first coordination shell are reported in Table 2 as well as the interatomic distance, R, the coordination number, N, and the Debye-Waller factor, σ^2. It is worth noting that:

– in the Er:$LiNbO_3$ crystals the mean number of oxygen atoms around Er varies from 7.1 to 8.7, being always higher than in the Er_2O_3 crystal, where each Er is surrounded by 6 O atoms.
– In the ion-exchanged samples the erbium – oxygen interatomic distance (2.32÷2.36 Å) is always longer than that observed in the Er_2O_3 standard (2.27 Å).

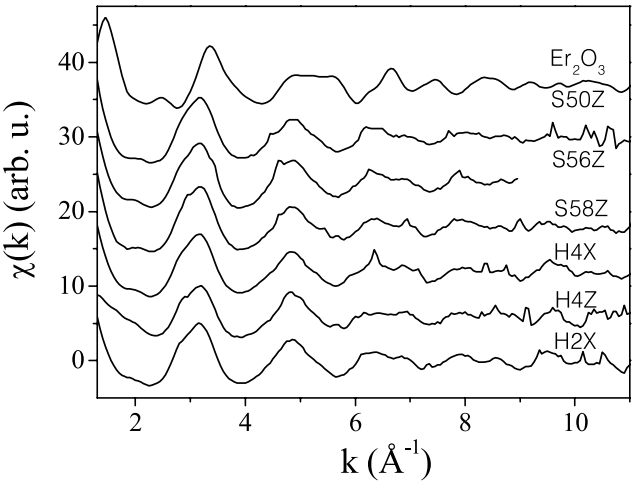

Fig. 3. Er L_{III}-edge EXAFS spectra for the ion-exchanged samples recorded in fluorescence mode and compared to that one of Er_2O_3 crystalline powder.

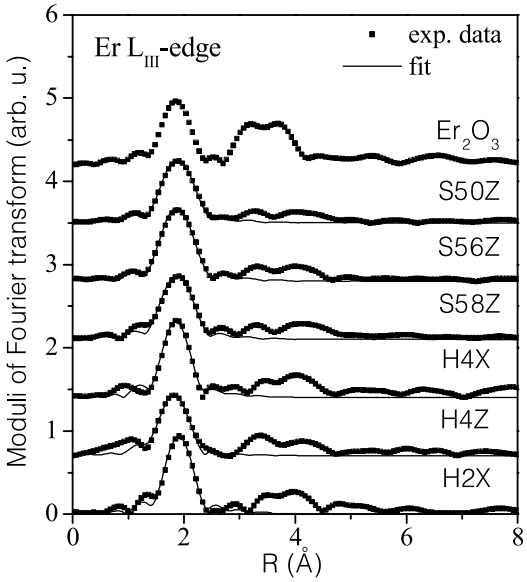

Fig. 4. Moduli of Fourier transform of k^3-weighted EXAFS spectra (dots: experimental data, solid line: fit), compared with that one for Er_2O_3 crystalline powder at Er L_{III}-edge. The EXAFS spectra were transformed in the 2–9 $Å^{-1}$ k-range.

– The Debye-Waller factors are generally larger in the exchanged samples with respect to the Er_2O_3 standard.

Concerning the role played by the different processing parameters:

– Higher erbium sulphate percentages in the bath composition lead to an increase of the first shell distance.
– The exchange time seems to favor only the in-depth incorporation of the dopant without promoting a significant structural rearrangement (compare S50Z and S58Z).

Table 2. Interatomic distance R, coordination number N and Debye-Waller factor σ^2 resulting from the XFY EXAFS analysis. For the Er_2O_3 standard, N is fixed to the crystallographic value, while R and σ^2 resulted from fitting.

Sample	R(Å)	N	$\sigma^2(\times 10^{-4}$Å$^2)$
Er_2O_3	2.27 ± 0.02	6 (fixed)	33 ± 6
S50Z	2.36 ± 0.02	7.7 ± 1.1	59 ± 12
S56Z	2.36 ± 0.02	8.7 ± 1.3	54 ± 11
S58Z	2.35 ± 0.02	7.9 ± 1.4	66 ± 27
H2X	2.36 ± 0.02	7.5 ± 1.5	44 ± 24
H4X	2.33 ± 0.02	7.1 ± 1.3	40 ± 21
H4Z	2.32 ± 0.02	8.3 ± 2.1	90 ± 36

– In the Z-cut samples the coordination numbers and the Debye-Waller factors are smaller than in the X-cut ones (see H4X and H4Z samples).
– In the Z-cut samples the Debye-Waller factor is smaller (of about 30%) when a slow heating rate is used. A slow heating rate seems to favor the local order.

Whether Er occupies the lithium or niobium site, after the ion exchange process takes place, is a critical point that, to our knowledge, has not been studied yet. In the case of pure congruent $LiNbO_3$ crystals, the first neighbors for both Li and Nb site are O atoms, at about 2 Å. Moreover for the Li site the second next neighbors are four Nb atoms at 3.04 Å, then three Nb at 3.38 Å and 3.92 Å, while for the Nb site they are six Nb at 3.76 Å [15]. The possible contribution of lithium to the EXAFS spectra can be ignored because of the very low back- scattering amplitude. To find out the site of Er atoms is therefore mandatory to extend the fit of the moduli of Fourier transform up to 4.5 Å and to investigate the contribution at higher value of R. It emerges that all the spectra can be fitted by assuming that in second and third shell Er coordinates oxygen atoms. The results of the fitting procedure show that the values of coordination distances of Er-O second shell vary between 3.75 Å to 3.80 Å (±0.03 Å) and Er-O third shell between 4.58 Å and 4.65 Å (±0.05 Å) for the different samples. The local environment of Er atoms in the crystal is made of O atoms as in the Er_2O_3 case but with longer coordination distances of second and third shell. As no contribution of Nb atoms was found within 4.5 Å, we can assert that the Er atoms are not in the Li site nor in the Nb one. The fact that Er does not occupy a Li or Nb site is worth noting: although the ion exchange process involves very complex mechanism, erbium environment in the ion exchanged samples is similar to that observed in Er bulk doped samples grown by the Czochralski technique. In the last case, in fact, Er was found near Li site, displaced 0.46 Å in the c-direction and without damaging the order crystal structure [16–19].

3.2.2 Total electron yield detection mode

As already mentioned, the heating rate strongly influences the erbium profile shape into the substrate, especially in the first 0.2 μm layer. The open question was therefore to understand whether in this region a modification in local environment of Er ions could occur. For this reason we collected the EXAFS signal in TEY configuration, limiting the sampled depth to about 170 nm [20]. In XFY mode, in fact, the whole erbium-doped layer is probed, as the calculated attenuation length for 8 keV X-ray is about 25 μm [21].

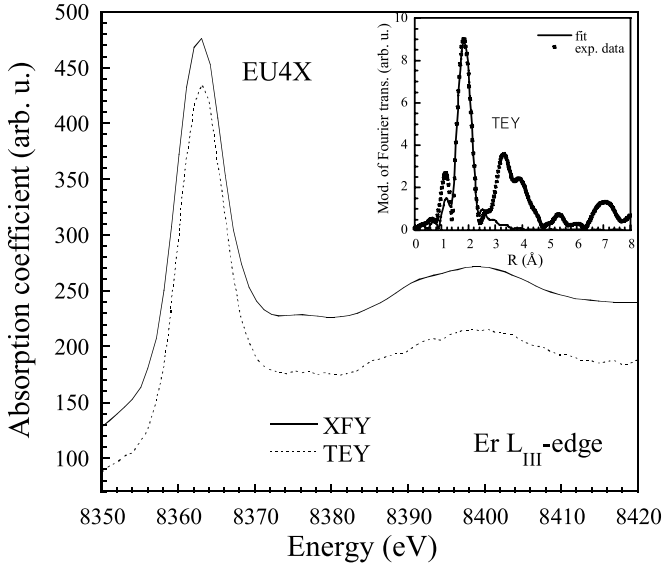

Fig. 5. XFY and TEY absorption spectra for the H4X sample. Inset: Moduli of Fourier transform of TEY EXAFS spectra for the H4X sample (dots: experimental data, solid line: fit); the EXAFS spectra were k^3-weighted, and transformed in the 2–9 Å^{-1} k-range.

In Figure 5 we compare the absorption coefficient for the H4X sample collected in both XFY and TEY modes and in the inset we report the TEY Fourier transform moduli, together with the relative fit. The results of the TEY EXAFS analysis for the first shell fit indicate that Er is surrounded by (7.4 ± 1.3) oxygen atoms at a distance equal to (2.33 ± 0.02) Å, and the Debye-Waller factor is $(44 \pm 22) \times 10^{-4}$ Å^2. First shell fitting results of XFY and TEY spectra are compatible within the experimental errors suggesting that no significant differences can be detected in the erbium local environment in the near surface layer.

4 Conclusions

Lithium niobate crystals doped with Erbium by the ion exchange process were studied by means of extended X-ray absorption fine structure (EXAFS) spectroscopy and secondary ion mass spectrometry (SIMS). From the compositional analysis we have found that the doping process can be explained in terms of erbium-lithium exchange mechanism. The erbium in-depth concentration profile strongly depends on the preparation parameters, especially on the heating rate used to melt the starting bath composition.

EXAFS results, however, evidenced that erbium incorporation cannot be described as a simple replacement process, since after the exchange, the erbium atoms are not located in the lithium sites. The process involves a reordering of the local environment due to the different valence state and dimension of the dopant ions with respect to the matrix elements. In the exchanged $LiNbO_3$ crystal, erbium is surrounded by three shells of oxygen atoms, but with Er-O atoms distances longer and coordination numbers greater than expected in pure Er_2O_3 matrix. It is worth noting that only small differences in the erbium local environment were found for different preparation conditions. Moreover, TEY analysis showed that there are no significant differences in the local environment of erbium atoms in the outmost layer (about two hundreds nm thick) with respect to the full exchanged layer. The difference in the SIMS profile in the exchanged samples when different heating rates are employed, might be ascribed to the erbium concentration in the outmost layer. When a fast heating rate is employed, a rapid exchange of Li ions occurs: the erbium concentration reaches a saturation value, forming a buffer layer that replaces the molten salts as source of erbium ions for the in-depth diffusion. When a slow heating rate is used, instead, the erbium content at the surface never reaches the saturation value it is only the molten salts to provide further erbium ions for the exchange process.

References

1. A. Polman, J. Appl. Phys. **82**, 1 (1997)
2. M.P. Hehlen, N.J. Cockroft, T.R. Gosnell, Phys. Rev. B **56**, 9302 (1997)
3. I. Baumann, R. Brinkmann, M. Dinand, W. Sohler, L. Beckers, Ch. Buchal, M. Fleuster, H. Holzbrecher, H. Paulus, K.H. Mller, Th. Gog, O. Witte, H. Stolz, W. von der Osten, Appl. Phys. A **64**, 33 (1997)
4. R. Brinkmann, I. Baumann, M. Dinand, W. Sohler, H. Suche, IEEE J. Quantum Electron. **30**, 2356 (1994)
5. I. Baumann, R. Brinkmann, M. Dinand, W. Sohler, and S. Westenhfer, IEEE J. Quantum Electron. **32**, 1695 (1996)
6. Yu.N. Korkishko, V.A. Fedorov, *Ion exchange in single crystals for integrated optics and optoelectronics* (Cambridge International Science Publishing Press, 1999)
7. C. Sada, E. Borsella, F. Caccavale, F. Gonella, F. Segato, Yu.N. Korkishko, V. Fedorov, T.V. Morozova, G. Battaglin, R. Polloni, App. Phys. Lett. **72**, 3431 (1998)
8. F. Caccavale, C. Sada, F. Segato, J. Non-Cryst. Solids **245**, 135 (1999)
9. F. Caccavale, C. Sada, F. Segato, B. Allieri, L.E. Depero, L. Sangaletti, V.A. Fedorov, Yu.N. Korkishko, T.V. Morozova, J. Non-Cryst. Solids **280**, 156 (2001)
10. J. Garcia Sol, Physica Scripta T **55**, 30 (1994)
11. P.A. Lee, P.H. Citrin, P. Eisenberger, B.M. Kincaid, Rev. of Mod. Phys. **53**, 769 (1981)
12. S. Pascarelli, F. Boscherini, F. D'Acapito, J. Hrdy, C. Meneghini, S. Mobilio, J. Synchr. Rad. **3**, 147 (1996)
13. A.L. Ankudinov, B. Ravel, J.J. Rehr, S.D. Conradson, Phys. Rev. B **58**, 7565 (1998)
14. C. Sada, F. Caccavale, F. Segato, B. Allieri, L.E. Depero, Optical Materials **19**, 23 (2002)
15. C. Mignotte, A. Traverse, P. Moretti, M. Monchanin, Nucl. Instum. and Meth. B **120**, 81 (1996)
16. Th. Gog, M. Griebenow, G. Materlik, Phys. Lett. A **18**, 417 (1993)
17. D.M.B.P. Milori, I.J. Moares, A.C. Hernandes, R.R. de Souza, M. Siu Li, M.C. Terrile, Phys. Rev. B **51**, 3206 (1995)
18. Th. Nolte, Th. Pawlik, J.M. Spaeth, Solid State Comm. **104**, 535 (1997)
19. A. Lorenzo, H. Jaffrezic, B.Roux, G.Boulon, J. Garci-Sol, Appl. Phys. Lett. **67**, 3735 (1995)
20. A. Erbil, G.S. Cargill III, R. Frahm, R.F. Boheme, Phys. Rev. B **37**, 2450 (1988)
21. B.L. Henke, E.M. Gullikson, J.C. Davis, *X-ray interactions: photoabsorption, scattering, transmission, and reflection at E=50–30000 eV, Z=1–92*, Atomic Data and Nuclear Data Tables Vol. **54**, 181–342 (1993)